

Dynamical shift condition for unequal mass black hole binaries

Doreen Müller, Jason Grigsby, Bernd Brügmann

Theoretical Physics Institute, University of Jena, 07743 Jena, Germany

(Dated: August 19, 2021)

Certain numerical frameworks used for the evolution of binary black holes make use of a gamma driver, which includes a damping factor. Such simulations typically use a constant value for damping. However, it has been found that very specific values of the damping factor are needed for the calculation of unequal mass binaries. We examine carefully the role this damping plays, and provide two explicit, non-constant forms for the damping to be used with mass-ratios further from one. Our analysis of the resultant waveforms compares well against the constant damping case.

PACS numbers: 04.25.D-, 04.25.dg, 04.25.Nx

I. INTRODUCTION

The ability to simulate the final inspiral, merger, and ring-down of black hole binaries with numerical relativity [1–3] plays a key role in understanding a source of gravitational waves that may one day be observed with gravitational wave detectors. While initial simulations focused on binaries of equal-mass, zero spin, and quasi-circular inspirals, there currently is a large effort to explore the parameter space of binaries, e.g. [4–7]. A key part of studying the parameter space is to simulate binaries with intermediate mass-ratios.

To date, the mass ratio furthest from equal masses that has been numerically simulated is 10:1 [8, 9]. These simulations use the Baumgarte-Shapiro-Shibata-Nakamura (BSSN) formulation [10–12] with 1+log slicing, and the $\bar{\Gamma}$ driver condition for the shift [13, 14]. In [8], it was noted that the stability of the simulation is sensitive to the damping factor, η , used in the $\bar{\Gamma}$ driver condition,

$$\partial_0^2 \beta^i = \frac{3}{4} \partial_0 \bar{\Gamma}^i - \eta \partial_0 \beta^i. \quad (1)$$

Here, β^i is the shift vector describing how the coordinates move inside the spatial slices, $\partial_0 \equiv \partial_t - \beta^i \partial_i$, and $\bar{\Gamma}^i$ is the contraction of the Christoffel symbol, $\bar{\Gamma}_{jk}^i$, with the conformal metric, $\tilde{\gamma}^{jk}$.

The standard choice for η is to set it to a constant value, which works well even for the most demanding simulations as long as the mass ratio is sufficiently close to unity. In binary simulations, a typical choice is a constant value of about $2/M$, with M the total mass of the system. This choice, however, leads to instabilities for the mass ratio 10:1 simulation [8], although stability was obtained for $\eta = 1.375/M$. The value of η is chosen to damp an outgoing change in the shift while still yielding stable evolutions. As we will show, if η is too small, there are unwanted oscillations, and values that are too large lead to instabilities. By itself, this observation is not new, see e.g. [15–18]. The key issue for unequal masses is that, as evident from (1), the damping factor η has units of inverse mass, $1/M$. Therefore, the interval of suitable values for η depends on the mass of the black

holes. For unequal masses, a constant η cannot equally well accommodate both black holes. A constant damping parameter implies that the effective damping near each black hole is asymmetric since the damping parameter has dimensions $1/M$. For large mass ratios, this asymmetry in the grid can be large enough to lead to a failure of the simulations because the damping may become too large or too small for one of the black holes. To cure this problem, we need a position-dependent damping parameter that adapts to the local mass. In particular, we want it to vary such that, in the vicinity of the i^{th} puncture with mass M_i , its value approaches $1/M_i$.

A position-dependent η was already considered when the $\bar{\Gamma}$ driver condition was introduced [8, 19–22], but such constructions were not pursued further because for moderate mass ratios a constant η works well. Recently, we revived the idea of a non-constant η for moving puncture evolutions in order to remove the limitations of a constant η for large mass ratios. In [23], we constructed a position-dependent η using the the conformal factor, ψ , which carries information both about the location of the black holes, and about the local puncture mass. The form of η was chosen to have proper fall-off rates both at the punctures and at large distance from the binary. In [9], this approach was used successfully for mass ratio 10:1. (We note in passing that damping is useful in other gauges as well, e.g. in [24] the modified harmonic gauge condition includes position-dependent damping by use of the lapse function.)

In the present work, we examine one potential shortcoming of the choice of [23], which leads us to suggest an alternative type of position-dependent η . Using [23], we find large fluctuations in the values of that η , and this might lead to instabilities in the simulation of larger mass-ratio binary black holes. To address this, we have tested two new explicit formulas for the damping factor designed to have predictable behavior throughout the domain of computation. We find the new formulas to produce only small changes in the waveforms that diminish with resolution, and there is a great deal of freedom in the implementation. Independently of our discussion here, in [16] the stability issues for large η are explained, and a non-constant η is suggested (although not yet explored

in actual simulations), that, in its explicit coordinate dependence, is similar to one of our suggestions.

The paper is organized as follows. We first describe the reasons for the damping factor and some of the reasons for limiting its value in Sec II. In Sec. III, we discuss some previous forms of η that have been used. We also present two new definitions and why we investigated them. In Sec. IV, we find that these new definitions agree well with the use of constant η in the extracted gravitational waves for mass ratios up to 4:1. Finally, in Sec. V, we discuss further implications of this work.

II. MOTIVATION

In order to define a position-dependent form for η , it is important to determine what this damping parameter accomplishes in numerical simulations. For this reason, we examine the effects of running different simulations while varying η between runs. First we use evolutions of single non-spinning black-holes to identify the key physical changes. Then we examine equal-mass binaries to determine specific values desired in η at both large and small radial coordinates.

A. Numerics

For all the work in this paper, we have used the BAM computer code described in [17, 25, 26]. It uses the BSSN formalism with 1+log slicing and $\tilde{\Gamma}$ driver condition in the moving puncture framework [2, 27]. Puncture initial data [28] with Bowen-York extrinsic curvature [29] have been used throughout this work, solving the Hamiltonian constraint with the spectral solver described in [30]. For binaries, parameters were chosen using [31] to obtain quasi-circular orbits, while the parameters for single black holes were chosen directly. We extract waves via the Newman-Penrose scalar Ψ_4 . The wave extraction procedure is described in detail in [17]. We perform a mode decomposition using spin-weighted spherical harmonics with spin weight -2 , Y_{lm}^{-2} , as basis functions and calculate the scalar product

$$\Psi_4^{lm} = (Y_{lm}^{-2}, \Psi_4) = \int_0^{2\pi} \int_0^\pi \sin\theta d\theta d\varphi \overline{Y_{lm}^{-2}} \Psi_4. \quad (2)$$

We further split Ψ_4^{lm} into mode amplitude A_{lm} and phase ϕ_{lm} in order to cleanly separate effects in these components, $r_{\text{ex}} \cdot \Psi_4^{lm} = A_{lm} e^{i\phi_{lm}}$. In this paper, we focus on one of the most dominant modes, the $l = m = 2$ mode, and report results for this mode unless stated otherwise. The extraction radius used here is $r_{\text{ex}} = 90 M$.

B. Single, non-spinning puncture with constant damping

The damping factor, η , in Eq. (1), is included to reduce dynamics in the gauge during the evolution. To examine the problem brought up in the introduction, we compare results of a single, non-spinning puncture with mass M . We use a Courant factor of 0.5 and 9 refinement levels centered around the puncture. The resolution on the finest grid is $0.025 M$, and the outer boundary is situated at $256 M$. Varying the damping constant between $0.0/M$ and $4.5/M$, two main observations can be made. First, as designed, a non-zero η attenuates emerging gauge waves efficiently. Second, an instability develops for values of η that are too large.

Figs. 1, and 2 illustrate the first observation. Both figures show the x -component of the shift along the x -coordinate using $\eta \in \{0.0/M, 1.5/M, 3.5/M\}$. Apart

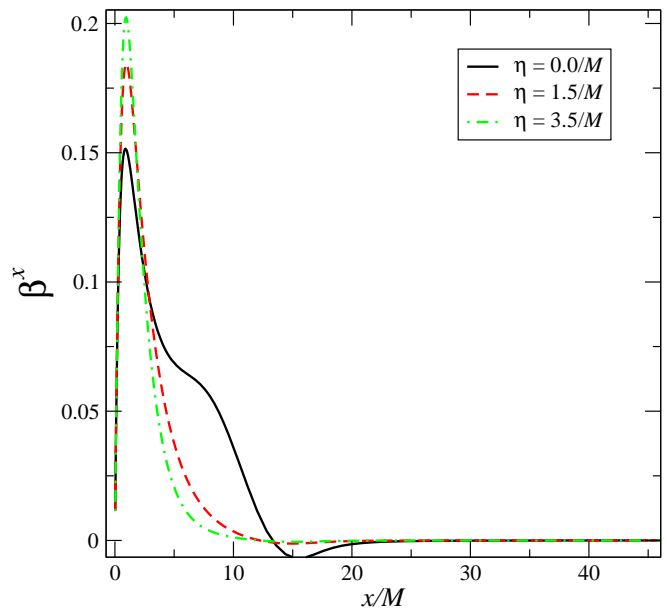


FIG. 1: The x -component of the shift, β^x , for a single non-spinning puncture of mass M at time $t = 15.2 M$. The three lines were taken for different values of the damping factor η . The solid line (black) is for $\eta = 0.0/M$. The dashed line (red) is for $\eta = 1.5/M$ and the dotted-dashed line (green) is for $\eta = 3.5/M$. This shows the beginning of a pulse in β^x for smaller values of η .

from the usual shift profile, Fig. 1 shows the beginnings of a pulse in the $\eta = 0.0/M$ case (solid line) at $x \approx 10 M$ after $15.2 M$ of evolution. Examining Fig. 2, where we zoom in at a later time, $t = 30.4 M$, one can see that the pulse has started to travel further out (solid line). Looking carefully, one can also see a much smaller pulse in the $\eta = 1.5/M$ line (dashed). Lastly, by examination, one can find almost no traveling pulse in the $\eta = 3.5/M$ curve (dotted-dashed line). The observed pulse in the shift travels to regions far away from the black hole and effects the gauge of distant observers. This might have

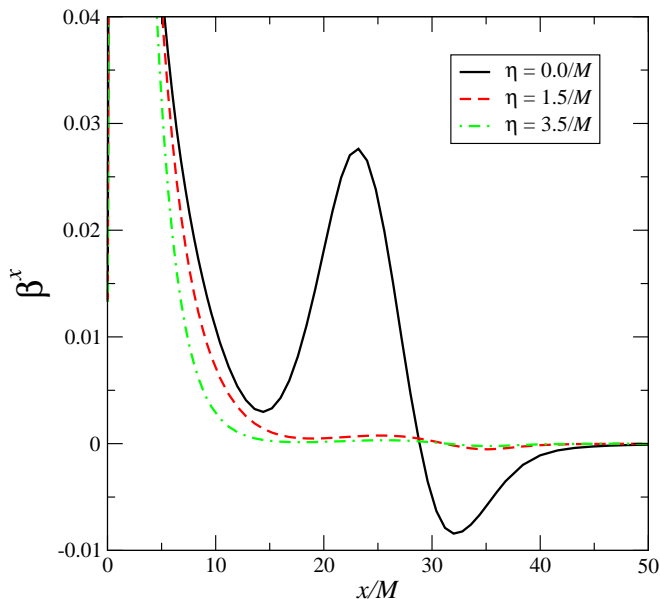


FIG. 2: The x -component of the shift, β^x , for a single non-spinning puncture of mass M at time $t = 30.4 M$. The three lines were taken for different values of the damping factor η with the same line type and color scheme as in Fig. 1. Here it is clear a pulse radiates outward in the shift with smaller values of η .

undesirable implications for the value of such numerical data when trying to understand astrophysical sources.

For values of η larger than $3.5/M$, an instability arises in the shift at larger radius. Fig. 3 shows the x -component of the shift vector using damping constants $\eta = 3.5/M$ (solid line), $\eta = 4.0/M$ (dashed line) and $\eta = 4.5/M$ (dotted-dashed line). The plots show an instability in simulations with $\eta > 3.5/M$ developing in β^i , which eventually leads to a failure of the simulations. Contrary to this, the simulation using $\eta = 3.5/M$ does not show this shift related instability. In test runs we found that by decreasing the Courant factor used, we could increase the value of the damping factor and still get stable evolutions. This agrees with [16] where it was shown that the gamma driver possesses the stiff property, which limits the size of the time-step in numerical integration based on the value of the damping.

Figures 1, 2, and 3 make clear how the choice of the damping factor affects the behavior of the simulations. The value we choose for η should be non-zero and not larger than $3.5/M$ to allow for effective damping and stable simulations. The exact cutoff value between stable and unstable simulations is not relevant here since the position dependent form we develop in Sec. III gives us the flexibility we need to obtain stable simulations.

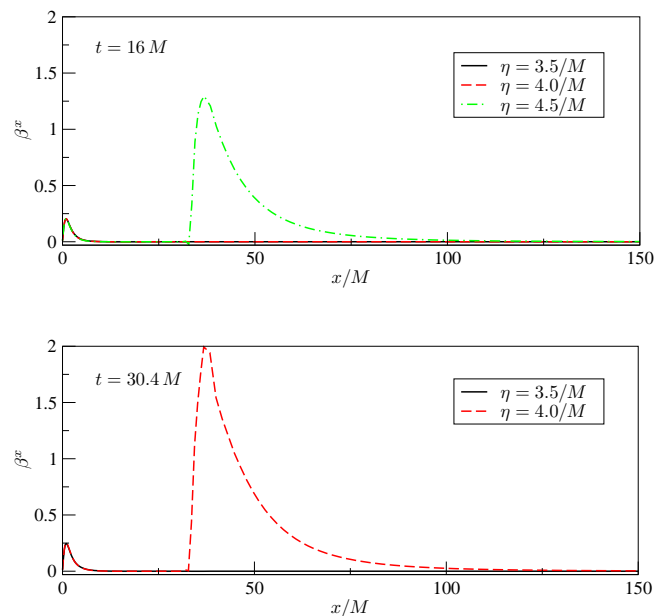


FIG. 3: The x -component of the shift vector in the x -direction for a single non-spinning puncture of mass M at times $t = 16.0 M$ and $t = 30.4 M$. The three different lines mark three values of the damping constant η . The solid line (black) is for $\eta = 3.5/M$, the dashed line (red) for $\eta = 4.0/M$ and the dotted-dashed line (green) for $\eta = 4.5/M$. At $t = 16 M$, the simulation using $\eta = 4.5/M$ develops an instability in the shift vector and fails soon afterward, the same happens for $\eta = 4.0/M$ at $t = 30.4 M$. In the simulation using $\eta = 3.5$, no such instability develops (not shown).

C. Equal mass binary with constant damping

To examine the effect of η on the extraction of gravitational waves, we compare the results from simulations of an equal mass binary with total mass M in quasi-circular orbits with initial separation $D = 10 M$, using $\eta \in \{0.0/M, 0.5/M, 2.0/M\}$. Again, the Courant factor is chosen to be 0.5 and we use, in the terminology of [17], the grid configuration $\chi[6 \times 56 : 5 \times 112 : 6]$ with a finest resolution of $0.013 M$. Here, the extraction radius r_{ex} is chosen to be $90 M$.

For vanishing η , we find a lot of noise in the the real part of the 22-mode of $r_{\text{ex}}\Psi_4$, shown in the solid curve of Fig. 4. A small, but non-vanishing η suffices to suppress this noise, as seen in the dashed curve of this figure. The dotted-dashed curve in this plot is the result for using the value $\eta = 2.0/M$. We see a difference in time between peak amplitudes of the three curves due to the change of coordinates that the alternation of η introduces. We did, however, find that by decreasing the Courant factor those differences between peak amplitudes summarily decreased.

To understand the noise in the waves for $\eta = 0.0/M$, we look at the shift vector at different times. The first panel of Fig. 5 shows the x -component of the shift over

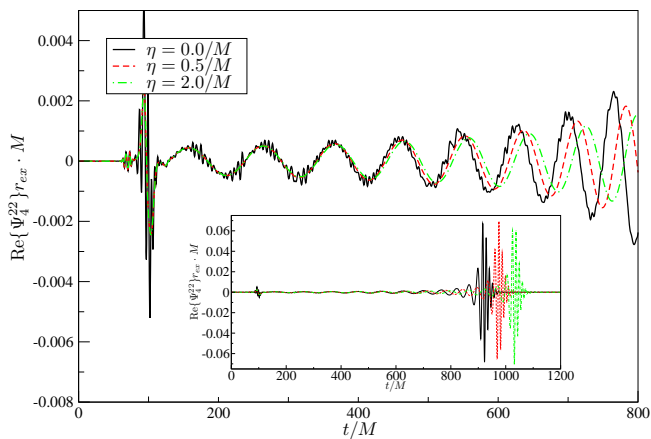


FIG. 4: Real part of the 22-mode of Ψ_4 over time for equal mass simulations using different values for η . The inset shows the full waveform until ringdown. The solid curves (black) are for $\eta = 0$, the dashed curve (red) mark $\eta = 0.5/M$ and the dotted-dashed curves (green) are for $\eta = 2.0/M$. Without damping in the shift, the extracted waves are noisy at times when the amplitude is still small (black, solid curve).

x , again for $\eta \in \{0.0/M, 0.5/M, 2.0/M\}$, shortly after the beginning of the simulation. The fourth panel shows the same at a time shortly before the merger, and the two panels in the middle represent intermediate times. We see clear gauge pulses in the earliest time panel for all three curves. We also observe the amplitude of this pulse decreasing with increasing η . As time goes on, the gauge pulse travels outwards as in the case for a single puncture in section II B. For vanishing η (solid line), the shift becomes more and more distorted, and the distortions do not leave the grid. For non-zero η , the amplitude of the gauge pulse decreases when traveling outwards, and the shape of β^x is not distorted. There is, compared to $\eta = 2.0/M$ (dotted-dashed line), only a small bump left in the $\eta = 0.5/M$ case (dashed line), that changes its shape slightly during the simulation, but does not travel to large distances from the punctures. The coordinates are disturbed in the case where no damping is used, and thus the noise in $r_{\text{ex}} \text{Re}\{\Psi_4^{22}\}$ is not surprising.

In this series, using a Courant factor of 0.5, we only obtained stable evolutions for $\eta < 3.5/M$ which agrees with the limits found in section II B. If we chose the value of η too large, the same kind of instability in the shift vector we found there develops in the equal mass case and the simulations fail. The failure occurs relatively early, before $50 M$ of evolution time, whereas the stable runs lasted about $1200 M$, including merger and ringdown (we stopped the runs after ringdown).

III. POSITION-DEPENDENT FORMS OF η

In section II B, we saw that a sufficient level of damping is needed to limit gauge dynamics, and too much damp-

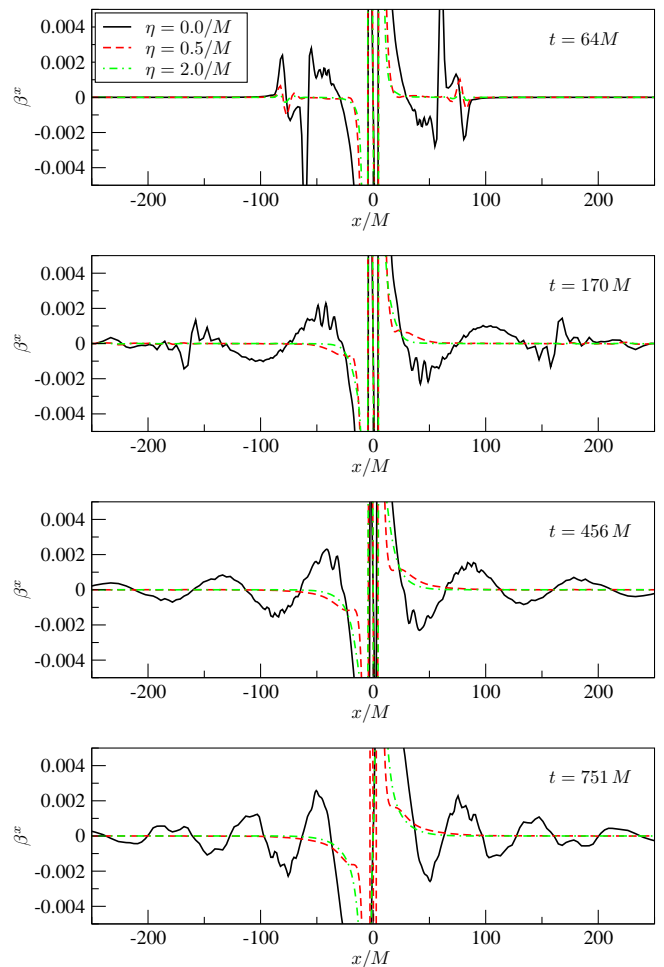


FIG. 5: x -component of the shift vector, β^x , for three different choices of η at four different times during the simulation. The physical system is the same as in Fig. 4. The merger takes place at approximately $t = 1000 M$. In the $\eta = 0/M$ case (black, solid curve), the shift vector is not damped and therefore, a pulse travels outwards and distorts the shift over the whole grid. The amplitude of this pulse is considerably damped when using a non-vanishing η and therefore the distortions are reduced. For $\eta = 0.5/M$ (red, dashed curve), there are still small bumps traveling out which are reduced by using $\eta = 2/M$ (green, dotted-dashed curve).

ing can lead to numerical instabilities. In section II C, we saw the positive effect that sufficient damping has on the resultant waveform for equal mass binaries. While we still need damping in the gamma driver in the unequal mass case, a constant value may not fulfill the requirements of limiting gauge dynamics and permitting stable evolutions. Rather, we need a definition for the damping that adjusts the value to the local mass-scale.

We will examine definitions, that naturally track the position, and mass of the individual black holes. The choice of η should provide a reasonable value both near the individual black holes, and at large distance from the binary. We will start by examining some previous

work, that has used non-constant forms of the damping parameter, and why it may be necessary to use other formulas. We will then present the two new formulas for η , which we designed for this work.

A. Previous dynamic damping parameters

A position dependent damping was introduced some years ago by the authors of [20], and was later used in [21]. That formula reads

$$\eta = \eta_{\text{punc}} - \frac{\eta_{\text{punc}} - \eta_{\infty}}{1 + (\psi - 1)^2} \quad (3)$$

with η_{punc} , η_{∞} being constants, and assuming $\psi = 1 + M_1/(2r_1) + M_2/(2r_2)$ (r_i is the distance to the i^{th} puncture). This formula was used to damp gauge dynamics while using excision for equal-mass head-on collisions. It has since been found that using the moving puncture framework allows for constant damping in the approximately equal mass case. We are looking for a formula which is suitable for the quasicircular inspiral of intermediate mass-ratio binaries.

Previously [23], we used the formula

$$\eta(\vec{r}) = \hat{R}_0 \frac{\sqrt{\tilde{\gamma}^{ij} \partial_i \psi^{-2} \partial_j \psi^{-2}}}{(1 - \psi^{-2})^2}, \quad (4)$$

for determining a position dependent damping coefficient instead of using a constant η . With \hat{R}_0 taken to be a unitless constant, it can be seen that Eq. (4) has units of inverse mass. The dependence on the BSSN variable, ψ , naturally tracks the position, and mass of the black holes. The application of Eq. (4) gave good values for the damping both at the punctures, and at the outer boundary, and was even found to somewhat decrease the grid-size of the larger black hole. The latter point could have positive effects on how the individual black holes are resolved on the numerical grid. It even had the additional effect of keeping the horizon shapes roughly circular, even close to merger - something that doesn't hold in the constant η case. Most importantly, the simulations remained stable, without significantly changing the gravitational waves. The formula was later used successfully for the 10:1 mass-ratio in [9].

Despite all this, Eq. (4) provides reason for concern. Fig. 6 shows the form of η using Eq. (4) for a non-spinning binary of equal mass in quasicircular orbits starting at a separation of $D = 10M$ at four different times in the simulation. As can be seen, noise travels out from the origin as time progresses. This leaves steady features on the form of η which could spike to higher and lower values than the range determined in Sec. II B. Additionally, these sharp features may lead to unpredictable coordinate drifts, and could, in some cases, affect the long-term stability of the simulation.

To illuminate the origin of the disturbances in $\eta(\vec{r})$, we looked at the development of $\eta(\vec{r})$ in simulations of

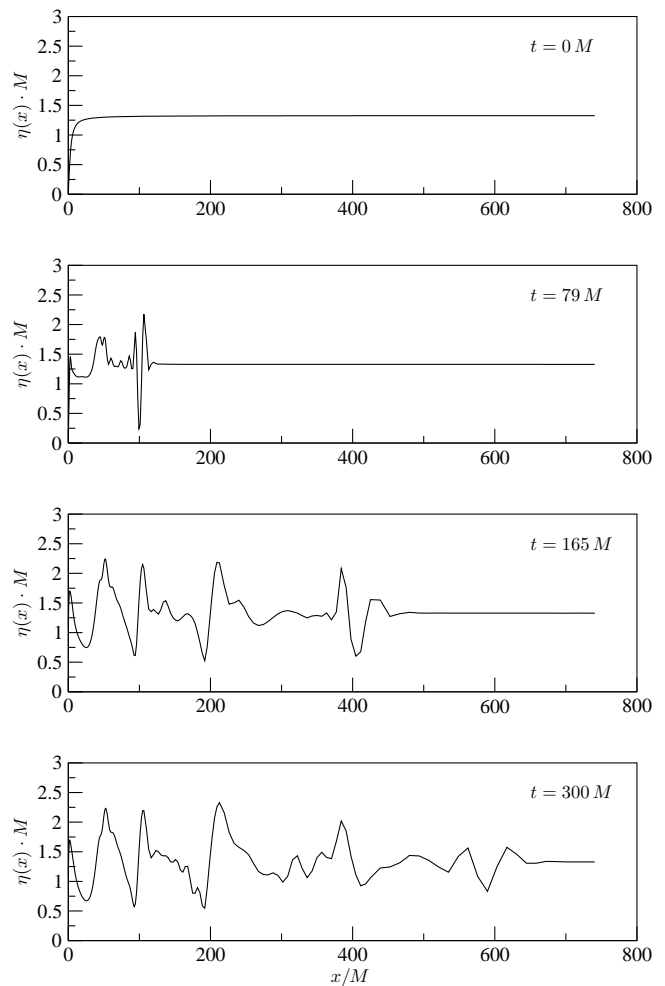


FIG. 6: Damping factor, η , along the x -axis using Eq. (4). The simulated configuration is an equal mass binary with initial separation $D = 10M$ and orbits lying in the (x, y) -plane. Shown are four different times during the simulation.

a single, non-spinning puncture, and a single, spinning puncture ($S_z/M^2 = 0.25$). The result for the spinning case is plotted in Fig. 7 at two different times over the x -axis. Again, we see a pulse traveling outwards. Only this time, it does not leave much noise on the grid. The fact that this pulse travels at a speed which is roughly 1.39 (in our geometric units where $c = G = 1$) in both the spinning and non-spinning scenario indicates that it is related to the gauge modes traveling at speed $\sqrt{2}$ in the asymptotic region where $\alpha \simeq 1$ (see [32] and [19] for a discussion of gauge speeds). In contrast to gauge pulses in the lapse, α , or shift vector, β^i , the pulse in $\eta(x)$ is amplified as it walks out. We found the same result in the single puncture simulation without spin. We believe the reason for this behavior is that as the distance to the puncture increases, the conformal factor, ψ , gets closer to unity. Therefore, the denominator in Eq. (4) approaches zero, and the gauge disturbances in the derivatives of ψ are magnified. We further observed reflections at the re-

finement boundaries as this pulse passes through them. This may explain the fluctuations in $\eta(x)$ shown in Fig. 6. While one could continue to fine-tune a formula dependent on the conformal factor to deal with these problems, we looked in a different direction to determine the form of the damping parameter.

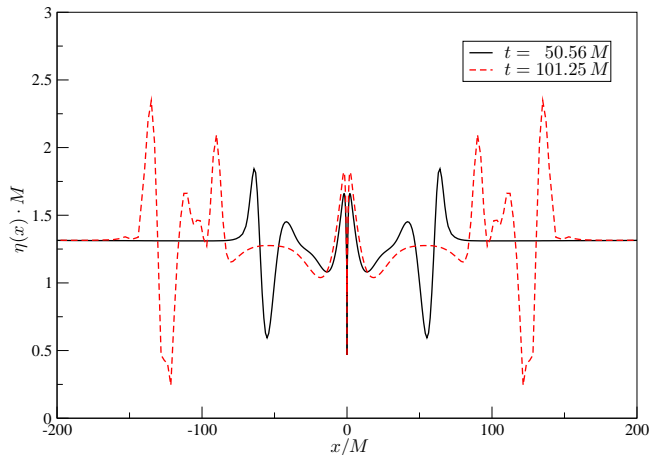


FIG. 7: Form of $\eta(\vec{r})$ for a single spinning puncture sitting at $x = 0$ using Eq. (4) after simulation time $t = 50.56 M$ (solid black line) and $t = 101.25 M$ (dashed red line) over x -direction.

B. Formulas for η with explicit dependence on the position and mass of the punctures

Since we always know the location of a puncture, and we know what its associated mass, we chose a form of damping that uses this local information throughout the domain. To address the demands and concerns discussed in Section II and III A, we designed two position-dependent forms of η . The two forms we tested are

$$\eta(\vec{r}) = A + \frac{C_1}{1 + w_1 (\hat{r}_1^2)^n} + \frac{C_2}{1 + w_2 (\hat{r}_2^2)^n}, \quad (5)$$

and

$$\eta(\vec{r}) = A + C_1 e^{-w_1 (\hat{r}_1^2)^n} + C_2 e^{-w_2 (\hat{r}_2^2)^n}. \quad (6)$$

In Eqs. (5) and (6), w_1 and w_2 are required to be positive, unitless parameters which can be chosen to change the width of the functions. The power n is taken to be a positive integer which determines the fall-off rate. The constants A , C_1 , and C_2 are then chosen to provide the desired values of η at the punctures, and at at infinity. Lastly, \hat{r}_1 and \hat{r}_2 are defined as $\hat{r}_i = \frac{|\vec{r}_i - \vec{r}|}{|\vec{r}_i - \vec{r}_2|}$, where i is either one or two, and \vec{r}_i is the position of the i 'th black hole.

The definition of \hat{r}_i is chosen to naturally scale the fall-off to the separation of the black holes. w_1 , w_2 , and n can be chosen to change the overall fall-off. Our work focuses

on the choice $w_1 = w_2 = w$ and $n = 1$. Following [23], we construct the damping factor to have units of inverse mass. We choose $A = 2/M_{tot}$, where $M_{tot} \equiv M_1 + M_2$ is defined as the sum of the irreducible masses. We then take $C_i = 1/M_i - A$. It is then evident that both Eqs. (5) and (6) will give a constant value of $\eta = 2/M_{tot}$ in the equal mass case.

We designed the two formulas for η in order to test the value of using fundamentally different functions. In our simulations, we found little noticeable difference in the application of one compared to the other. In the absence of such a difference, it becomes more beneficial to use Eq. (5), as Gaussians are computationally more expensive. It should be pointed out that Eq. (5) is very similar to Eq. (13) suggested in [16], and we believe the following results are very similar to what would be found using that form for the damping. Going into the present work, we have no ansatz which might suggest these forms of damping yield wave forms which are any better than the use of any previous form of η . However, as will be seen in the results sections, the waveforms we get from unequal mass binaries show noticeable improvement over the constant η case.

IV. RESULTS

For data analysis purposes, we are mainly interested in the properties of the emitted gravitational waves of the black hole binary systems under study. Hence, it is important to check how the changes in the gauge alter the extracted waves. In the context of gravitational wave extraction, Ψ_4 is only first order invariant under coordinate transformations. In addition, we have to chose an extraction radius r_{ex} for the computation of modes, which is also coordinate dependent. Although the last point can be partly addressed by extrapolation of $r_{ex} \rightarrow \infty$, it is a priori not clear how much a change of coordinates affects the gravitational waves. Furthermore, a change of coordinates implies an effective change of the numerical resolution, and for practical purposes we have to ask how much waveforms differ at a given finite resolution.

A. Waveform comparison using formula (5)

The results in the following section refers to the use of Eq. (5). We compare numerical simulations using three different grid configurations, which correspond to three different resolutions. In the terminology of [17], the grid set-ups are $\phi[5 \times 64 : 7 \times 128 : 5]$, $\phi[5 \times 72 : 7 \times 144 : 5]$, and $\phi[5 \times 80 : 7 \times 160 : 5]$, which corresponds to resolutions on the finest grids of $3M/320$ ($N = 64$), $M/120$ ($N = 72$) and $3M/400$ ($N = 80$), respectively. When referring to results from different resolutions, we will from here on use the number of grid points on the finest grid, N , to distinguish between them. In this subsection, we use $w_1 = w_2 = 12$ and $n = 1$ in Eq. (5). As test system we

use an unequal mass black hole binary with mass ratio $m_2/m_1 = 4$ and an initial separation of $D = 5M$ without spins in quasi-circular orbits.

For orientation, Fig. 8 shows the amplitude of the 22-mode, A_{22} , computed with the standard gauge $\eta = 2/M$ (displayed as solid lines) and with the new $\eta(\vec{r})$ using Eq. (5) (displayed as non-solid lines). The three different colors correspond to the three resolutions. The inset shows a larger time range of the simulation, while the main plot concentrates on the time frame around merger. The plot gives a course view of the closeness of the results we obtain with standard and new gauges.

In Fig. 9, we plot the relative differences between the amplitudes at low and medium (solid lines), and medium and high resolution (non-solid lines) obtained with $\eta = 2/M$ (light gray lines) as well as $\eta(\vec{r})$ (Eq. (5)) (black lines). Here, we find the maximum error between the low and medium resolution of the series using $\eta = 2/M$ amounts to about 12% (solid gray curve). Between medium and high resolution (dashed gray curve), we find a smaller relative error, but it still goes up to 7% at the end of the simulation. Employing Eq. (5), the maximum amplitude error between low and medium resolution (solid black line) is only about 4%, and therefore even smaller than the error between medium and high resolution for the constant damping case. Between medium and high resolution, the relative amplitude differences for Eq. (5) are in general smaller than the ones between low and medium resolution, although the maximum error is comparable to it (dot-dashed black line).

We repeat the previous analysis for the phase of the 22-mode, ϕ_{22} . Again, we compare the errors between resolutions in a fixed gauge. Figure 10 shows that the error between lowest and medium resolution using $\eta = 2/M$ (solid gray line) grows up to about 0.31 radians. For the differences between medium and high resolution (dashed line) we find a maximal error of 0.2 radians for $\eta = 2/M$. For $\eta(\vec{r})$ following Eq. (5), the phase error between low and medium resolution is only about 0.19 radians (solid black line) and decreases to 0.1 radians between medium and high resolution (dot-dashed line). Again, employing the position dependent form of η , Eq. (5), the error between lowest and medium resolution is lower than the one we obtain for constant η between medium and high resolution. The results for amplitude and phase error suggest that we can achieve the same accuracy with less computational resources using a position-dependent $\eta(\vec{r})$.

B. Waveform comparison using formula (6)

We repeated the analysis of Sec. IV A with the waveforms we obtain using Eq. (6) (with $w_1 = w_2 = 12$ and $n = 1$). We use the same initial conditions (mass ratio 4 : 1, $D = 5M$, no spins), and compare the amplitudes and phases of the 22-mode of Ψ_4 with the results of the $\eta = 2/M$ -runs. The grid configurations remain the same.

The results are very similar to the ones we obtained in

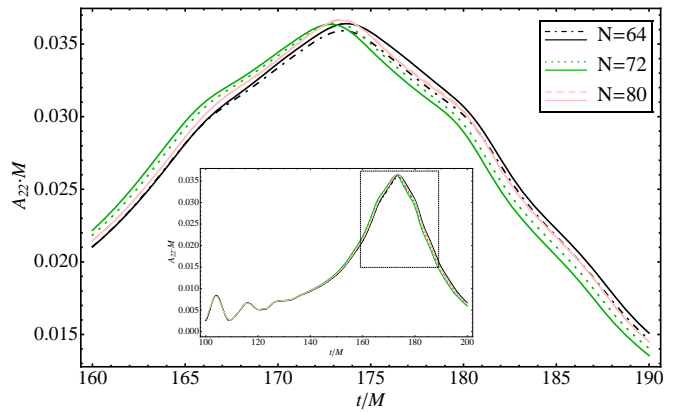


FIG. 8: Amplitude of the 22-mode of Ψ_4 of a binary with mass ratio 4:1 and initial separation $D = 5M$. The different colors correspond to three different resolutions according to the grid setup described in the text. The solid lines are results for $\eta = 2/M$, the dashed, dotted and dot-dashed ones are for $\eta(\vec{r})$ (Eq. (5)). The inset shows the simulation from shortly after the junk radiation passed, in the main plot we zoom into the region of highest amplitude (near the merger).

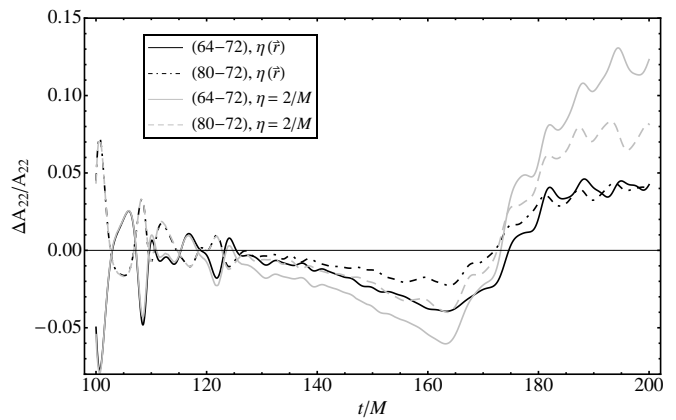


FIG. 9: Relative differences of the amplitude of the 22-mode of Ψ_4 between resolutions $N = 64$ and $N = 72$ (gray solid curve) as well as $N = 72$ and $N = 80$ (gray dashed curve) when using $\eta = 2/M$. The same for $\eta(\vec{r})$ (Eq. (5)) between $N = 64$ and $N = 72$ (black solid curve) and $N = 72$ and $N = 80$ (black dot-dashed curve). The physical situation is the same as in Fig. 8. The maximum differences are above 10%, comparing low and medium resolution of the constant η simulations (gray solid line).

Figs. 9 and 10, and we therefore do not show them here. Although Eqs. (5) and (6) result in different shapes for $\eta(\vec{r})$, Ψ_4^{22} is very similar. Therefore, the comparison to $\eta = 2/M$ naturally gives very similar results, too. The phase differences between results from Eqs. (5) and (6) at a given resolution are shown in Fig. 11. These are, with a maximum phase error of 0.004 radians, very small compared to the phase errors between resolutions, which, at minimum, are about 0.1 radian (see Fig. 10). Fig. 12 compares the phase error between low and medium (solid

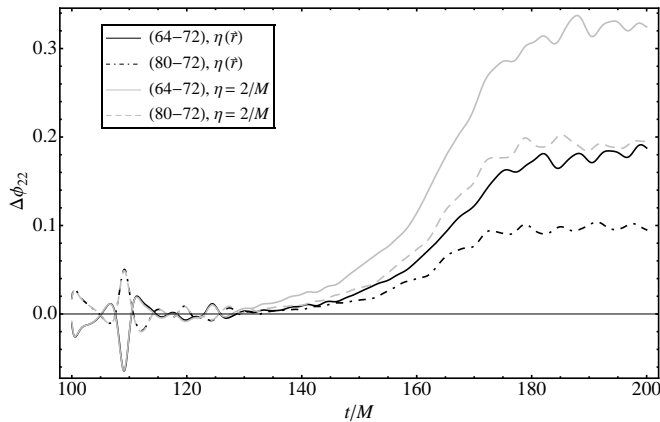


FIG. 10: Phase differences between lowest and medium resolution for the series using $\eta = 2/M$ (solid gray line) and $\eta(\bar{r})$ (Eq. (5)) (solid black line) as well as between medium and high resolution for $\eta = 2/M$ (dashed gray line) and for $\eta(\bar{r})$ (Eq. (5)) (dot-dashed black line). The physical situation is the one of Fig. 8.

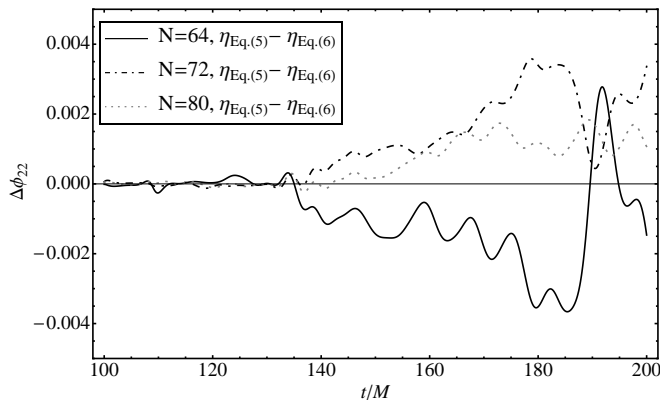


FIG. 11: Phase differences between waveforms obtained with Eq. (5) and Eq. (6) in three different resolutions (solid, dashed, dotted-dashed lines) for mass ratio 4:1, $D = 5 M$.

lines), and medium and high resolution (dotted-dashed and dashed line) of Eq. (6) (gray) to the ones of Eq. (5) (black). For comparison, the error between medium and high resolution is also plotted for Eq. (4) in this figure (dotted line). The plot indicates that the errors between resolutions are in good agreement for the different position dependent formulas of η .

C. Behavior of the shift vector

In [23], we found an unusual behavior of the shift vector. This is illustrated in Fig. 13, where we plot the x -component of the shift, β^x , in the x -direction after $160 M$ of evolution (this means approximately $80 M$ after merger) for all four versions of the damping constant we used for comparison in this paper before, and for the same binary configuration as the one used in Secs. IV A

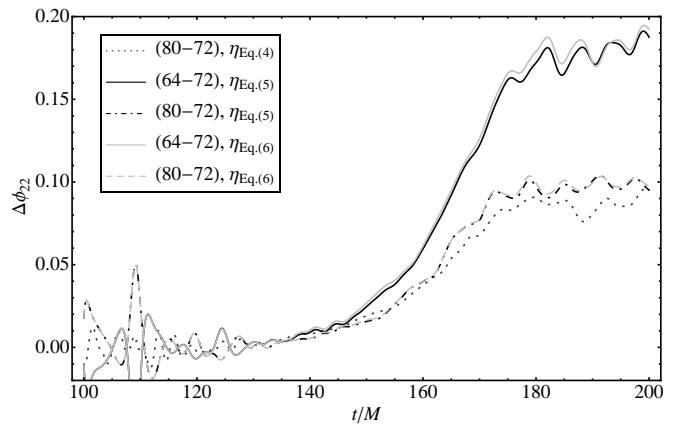


FIG. 12: Phase difference between waveforms at low and medium resolution (solid lines) and medium and high resolution (dotted-dashed and dashed line) using either Eq. (5) (black lines) or Eq. (6) (gray lines) for mass ratio 4:1, $D = 5 M$. For comparison, we also show the phase difference obtained with Eq. (4) between medium and high resolution (dotted line).

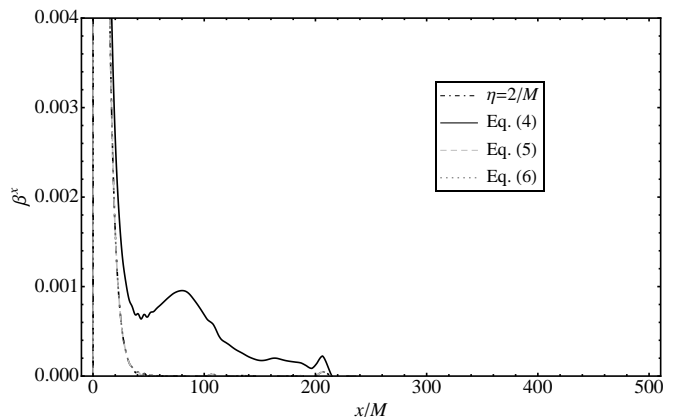


FIG. 13: x -component of the shift vector in x -direction after $160 M$ of evolution of the system with mass ratio 4 : 1 and $D = 10 M$. The black, dot-dashed line refers to the use of a constant damping η , while the black, solid line uses Eq. (4). The gray, dashed line is for the use of Eq. (6) and the gray, dotted one for Eq. (5). Except for the constant η (black, dot-dashed line), the results in this plot are indistinguishable.

and IV B. Like in [23], we find that using Eq. (4) results in a shift which falls off to zero too slowly towards the outer boundary, and which develops a “bump” (black, solid line), while the constant damping case (black, dot-dashed line) falls off to zero quickly. Employing Eqs. (5) or (6) avoids this undesirable feature. After merger, the shift falls off to zero when going away from the punctures as it does in the constant damping case (gray dashed and dotted lines). Using Eq. (5) or (6) prevents unwanted coordinate drifts at the end of the simulations.

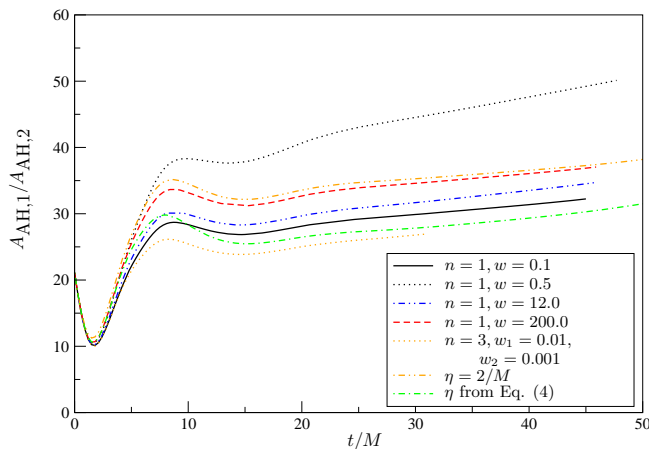


FIG. 14: Shown is the time dependence of the ratio between the coordinate areas of the apparent horizons of both black holes in a simulation with mass ratio 4 : 1 with initial separation $D = 5 M$. The black, blue and red lines use $\eta(\vec{r})$, Eq. (5) with varying values of the width parameter w . The orange line (dash-dot-dot) uses the constant damping $\eta = 2/M$ and the green (dash-dot) one refers to the result of [23] with Eq. (4). Using Eq. (5), the coordinate areas can be varied with respect to each other depending on the choice of w . A ratio of 1 means the black holes have the same size on the numerical grid.

V. DISCUSSION

In this work, we examined the role that the damping factor, η , plays in the evolution of the shift when using the gamma driver. In particular, we examined the range of values allowed in various evolutions, and what effects showed up because of the value chosen. We then designed a form of η for the evolution of binary black holes which provides appropriate values both near the individual punctures and far away from them with a smooth transition in between.

In Sec. IV, we directly examined the waveforms for the case using Eq. (5), where $w_1 = w_2 = 12$ and $n = 1$. While the form of η is predictable, and can be easily adjusted for stability, we also saw that the waveforms produced using this definition showed less deviation with increasing resolution than using a constant η . When examining the waveforms produced using Eq. (6), we found similar results. In the absence of a noticeable difference in the quality of the waveforms, Eq. (5) is computationally cheaper, and, as such, is our preferred definition for the damping.

We have already pointed out a certain freedom to pick parameters in Eqs. (5) and (6). We did perform some experimentation along this line where we varied $w = w_1 = w_2$ to see if we could get a useful effect of the coordinate size of the apparent horizons on the numerical grid. In [17, 33], it was noticed that the damping coefficient affects the coordinate location of the apparent horizon, and therefore the resolution of the black hole on

the numerical grid. Fig. 14 plots the ratio of the grid-area of larger apparent horizon to the smaller apparent horizon as a function of time for w -values of 0.1, 0.5 and for 200, all with $n = 1$. Also plotted is the relative coordinate size for the same binaries using a constant η in dashed, double-dotted line, and for using Eq. (4) in a blue dashed-dotted line. All the evolutions show an immediate dip, and then increase in the grid-area ratio during the course of the evolution. While a very low ratio was found using Eq. (4), the orange dotted line was later found for the choices of $n = 3$ with $w_1 = 0.01$ and $w_2 = 0.0001$ with Eq. (5). Due to this freedom in the implementation of our explicit formula for the damping, it may be possible to further reduce the relative grid size of the black holes. This effect could be important in easing the computational difficulty of running a numerical simulation for unequal mass binaries.

Having a form of η that leads to stable evolutions for any mass-ratio is an important step towards the numerical evolution of binary black holes in the intermediate mass-ratio. We believe the form given in Eq. (5) provides such a damping factor at a low computational cost, although the test results presented are limited to mass ratio 4 : 1. We plan to examine larger mass ratios in future work. The new method should allow binary simulations for mass ratio 10 : 1, or even 100 : 1. It remains to be seen whether other issues than the gauge are now the limiting factor for simulations at large mass ratios.

Acknowledgments

It is a pleasure to thank Zhoujian Cao and Erik Schnetter for discussions. This work was supported in part by DFG grant SFB/Transregio 7 “Gravitational Wave Astronomy” and the DLR (Deutsches Zentrum für Luft und Raumfahrt). D. M. was additionally supported by the DFG Research Training Group 1523 “Quantum and Gravitational Fields”. Computations were performed on the HLRB2 at LRZ Munich.

-
- [1] F. Pretorius, Phys. Rev. Lett. **95**, 121101 (2005), gr-qc/0507014.
- [2] M. Campanelli, C. O. Lousto, P. Marronetti, and Y. Zlochower, Phys. Rev. Lett. **96**, 111101 (2006), gr-qc/0511048.
- [3] J. G. Baker, J. Centrella, D.-I. Choi, M. Koppitz, and J. van Meter, Phys. Rev. Lett. **96**, 111102 (2006), gr-qc/0511103.
- [4] F. Pretorius (2007), arXiv:0710.1338v1 [gr-qc].
- [5] M. Hannam (2009), arXiv: 0901.2931 [gr-qc].
- [6] U. Sperhake, Lect. Notes Phys. **769**, 125 (2009).
- [7] B. Aylott, J. G. Baker, W. D. Boggs, M. Boyle, P. R. Brady, D. A. Brown, B. Brügmann, L. T. Buchman, A. Buonanno, L. Cadonati, et al., Class. Quant. Grav. **26**, 165008 (2009), arXiv: 0901.4399 [gr-qc].
- [8] J. A. González, U. Sperhake, and B. Brügmann, Phys. Rev. **D79**, 124006 (2009), arXiv: 0811.3952 [gr-qc].
- [9] C. O. Lousto, H. Nakano, Y. Zlochower, and M. Campanelli (2010), arXiv:1001.2316 [gr-qc].
- [10] M. Shibata and T. Nakamura, Phys. Rev. D **52**, 5428 (1995).
- [11] T. W. Baumgarte and S. L. Shapiro, Phys. Rev. D **59**, 024007 (1998), gr-qc/9810065.
- [12] T. Nakamura, K. Oohara, and Y. Kojima, Prog. Theor. Phys. Suppl. **90**, 1 (1987).
- [13] M. Alcubierre and B. Brügmann, Phys. Rev. D **63**, 104006 (2001), gr-qc/0008067.
- [14] M. Alcubierre, B. Brügmann, D. Pollney, E. Seidel, and R. Takahashi, Phys. Rev. D **64**, 061501 (2001), AEI-2001-021, gr-qc/0104020.
- [15] U. Sperhake (2006), gr-qc/0606079.
- [16] E. Schnetter (2010), arXiv: 1003.0859 [gr-qc].
- [17] B. Brügmann, J. A. González, M. Hannam, S. Husa, U. Sperhake, and W. Tichy, Phys. Rev. **D77**, 024027 (2008), gr-qc/0610128.
- [18] J. R. van Meter, J. G. Baker, M. Koppitz, and D.-I. Choi, Phys. Rev. D **73**, 124011 (2006), gr-qc/0605030.
- [19] M. Alcubierre, B. Brügmann, P. Diener, M. Koppitz, D. Pollney, E. Seidel, and R. Takahashi, Phys. Rev. D **67**, 084023 (2003), gr-qc/0206072.
- [20] M. Alcubierre, B. Brügmann, P. Diener, F. Herrmann, D. Pollney, E. Seidel, and R. Takahashi (2004), gr-qc/0411137, gr-qc/0411137.
- [21] Y. Zlochower, J. G. Baker, M. Campanelli, and C. O. Lousto, Phys. Rev. D **72**, 024021 (2005), gr-qc/0505055.
- [22] P. Diener, F. Herrmann, D. Pollney, E. Schnetter, E. Seidel, R. Takahashi, J. Thornburg, and J. Ventrella, Phys. Rev. Lett. **96**, 121101 (2006), gr-qc/0512108, URL <http://link.aps.org/abstract/PRL/v96/e121101>.
- [23] D. Müller and B. Brügmann (2009), arXiv: 0912.3125 [gr-qc].
- [24] L. Lindblom and B. Szilágyi, Phys. Rev. **D80**, 084019 (2009), arXiv: 0904.4873 [gr-qc].
- [25] S. Husa, J. A. González, M. Hannam, B. Brügmann, and U. Sperhake, Class. Quantum Grav. **25**, 105006 (2008), arXiv:0706.0740 [gr-qc].
- [26] B. Brügmann, W. Tichy, and N. Jansen, Phys. Rev. Lett. **92**, 211101 (2004), gr-qc/0312112.
- [27] J. G. Baker, J. Centrella, D.-I. Choi, M. Koppitz, and J. van Meter, Phys. Rev. Lett. **96**, 111102 (2006), gr-qc/0511103.
- [28] S. Brandt and B. Brügmann, Phys. Rev. Lett. **78**, 3606 (1997), gr-qc/9703066.
- [29] J. M. Bowen and J. W. York, Jr., Phys. Rev. D **21**, 2047 (1980).
- [30] M. Ansorg, B. Brügmann, and W. Tichy, Phys. Rev. D **70**, 064011 (2004), gr-qc/0404056.
- [31] B. Walther, B. Brügmann, and D. Müller, Phys. Rev. **D79**, 124040 (2009), arXiv: 0901.0993 [gr-qc].
- [32] C. Gundlach and J. M. Martin-Garcia, Phys. Rev. D **74**, 024016 (2006), gr-qc/0604035.
- [33] F. Herrmann, D. Shoemaker, and P. Laguna (2006), gr-qc/0601026.